JOURNAL OF APPLIED ELECTROCHEMISTRY 20 (1990) 405–417

Development of anodes for aluminium/air batteries — solution phase inhibition of corrosion

D. D. MACDONALD, C. ENGLISH
SRI International, Menlo Park, CA 94025, USA

Received 7 April 1989; revised 30 June 1989

The discharge characteristics of aluminium in inhibited and uninhibited 4 M KOH at 50° C have been explored. The performance of pure aluminium as a fuel is compared with that for two leading alloy fuels that had been evaluated in our previous work, Alloy BDW (Al–1Mg–0.1In–0.2Mn) and Alloy 21 (Al–0.2Ga–0.1In–0.1Tl). The inhibitors employed in this study, SnO_3^{2-}, $In(OH)_3$, BiO_3^{3-}, $Ga(OH)_4^-$, MnO_4^{2-}, and binary combinations thereof, are either present in Alloys BDW and 21 or have been investigated previously (SnO_3^{2-}). We found that potassium manganate (K_2MnO_4) and Na_2SnO_3 + $In(OH)_3$ are effective inhibitor systems, particularly at high discharge rates (400 mA cm^{-2}), but at low discharge rates only manganate offers a significant advantage in coulombic efficiency over the uninhibited solution. Alloy BDW exhibits a very low open circuit (standby) corrosion rate, but its coulombic efficiency under discharge, as determined by delineating the partial anodic and cathodic reactions, was found to be no better than that of aluminium in the same uninhibited solution. Alloy 21 was found to exhibit a comparable performance to Alloy BDW under open circuit conditions and a much higher coulombic efficiency at low discharge rates (100 mA cm^{-2}), but the performance of this alloy under high discharge rate conditions was not determined. Alloy 21 has the significant disadvantage that it contains thallium.

1. Introduction

Aluminium/air batteries are currently being developed for vehicular propulsion and as primary power sources for some stationary applications [1–24]. Regardless of the nature of the electrolyte (acidic, neutral or alkaline), these primary cells consist of an aluminium alloy anode and a unifunctional air cathode. The advantage this system offers over other metal/air batteries (for example, iron/air, zinc/air) are the very high theoretical energy density of the fuel [15], the unifunctional mode of operation of the air cathode (which ensures a longer life than that of the bifunctional counterpart), and the fact that the system is mechanically, rather than electrically, recharged. This latter feature is particularly important (although frequently ignored), because it should be possible to refuel an aluminium/air battery in a time comparable to that for an internal combustion engine (ICE), which is only a small fraction of that for electrically recharged (secondary) batteries such as iron/air and zinc/air. Accordingly, Al/air batteries (or fuel cells) are more suited to long-range, multiple refuelling operations than to short intracity excursions. The benign nature of the fuel and the near-ambient temperature of operation also render Al/air batteries suitable for some military and reserve applications.

To a large extent, the performance of an Al/air battery is determined by the electrochemistry and corrosion properties of the fuel. Pure aluminium is too reactive to be used directly, particularly in the uninhibited, highly alkaline electrolytes required for optimal performance of the air cathode. Consequently, considerable work has been reported on the development of dilute alloy fuels that have superior corrosion resistance under open circuit (standby) conditions and have acceptable discharge characteristics. Several promising alloys have been developed [22–27], but they are of limited practical application because they either contain toxic alloying elements (such as Tl) or are difficult to produce in a reproducible manner. Furthermore, the compositions of the alloys and the thermomechanical processing required to achieve optimal performance requires the establishment of special production facilities, which would be economically viable only if Al/air batteries came into widespread use because of either a shortage of petroleum fuels for ICEs or severe limitations placed on the burning of fossil fuels for environmental reasons.

An attractive alternative to alloy fuels is the possible use of solution-phase inhibitors to reduce the corrosion rate of an aluminium anode to an acceptable level. Accordingly, it might be possible to use scrap aluminium as fuel, in which case the cost of the fuel might have been partly or wholly defrayed by previous use. Furthermore, special alloying and thermomechanical processing facilities would not be required, because the anodes could be simply cast from the melted scrap. Solution-phase inhibition has been explored briefly in the past [1, 2], with the result that stannate has been added to the alkaline electrolyte of various experimental aluminium/air batteries. How-

0021-891X/90 $03.00 + .12

ever, no systematic studies of solution-phase inhibition have been reported.

In this paper, an evaluation of various inorganic oxyanions (SnO_3^{2-}, $Ga(OH)_4^-$, $In(OH)_3$, MnO_4^{2-}, BiO_3^{3-}, and combinations thereof) as inhibitors for the corrosion of pure aluminium (99.99%) in 4 M KOH at 50° C is presented. These ions were chosen because they are derived from metals that have been explored previously [22] as alloying additions and have been shown to influence the rate of corrosion of the alloy.

2. Experimental details

2.1. *Apparatus*

The electrochemical cell used to study the effects of solution-phase inhibition on aluminium is shown schematically in Fig. 1. The cell is made from clear polyvinyl chloride (PVC) sections bolted together to form a unit about 10 cm long that comprises both a test section and a monitoring section. The cell is placed in a flow loop (Fig. 2) with the electrolyte entering the test section at a flow rate of 0.023 l s^{-1} via a PTFE piston pump (Cole-Parmer Model 7149-10). The electrolyte reservoir is immersed in a constant temperature bath set at 50° ± 1° C. A calibrated thermocouple measures the temperature at the entrance to the test cell.

The working electrode for the test section consists of a 99.99% aluminium disc (3 mm long and 6 mm in diameter) connected to a thin aluminium rod using conducting silver epoxy. The sides of the disc and the epoxied connection were coated with lacquer to minimize crevice corrosion. After drying, the specimen was mounted in acrylic resin, and threaded to fit the work-

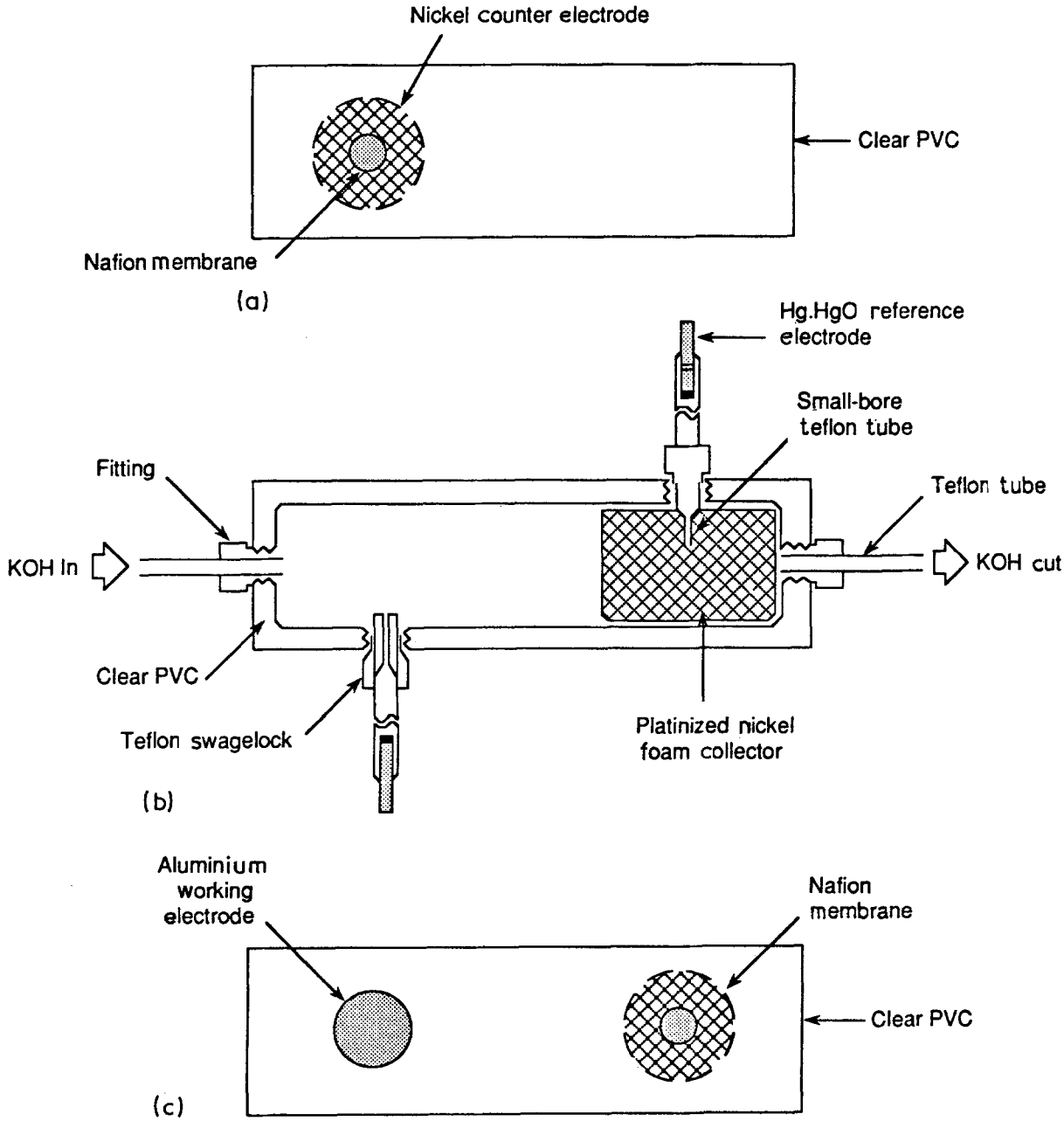

Fig. 1. Sections of electrochemical cell for polarization measurements of aluminium alloys. (Note: Outer sections (a) and (c) are bolted to inner section (b).)

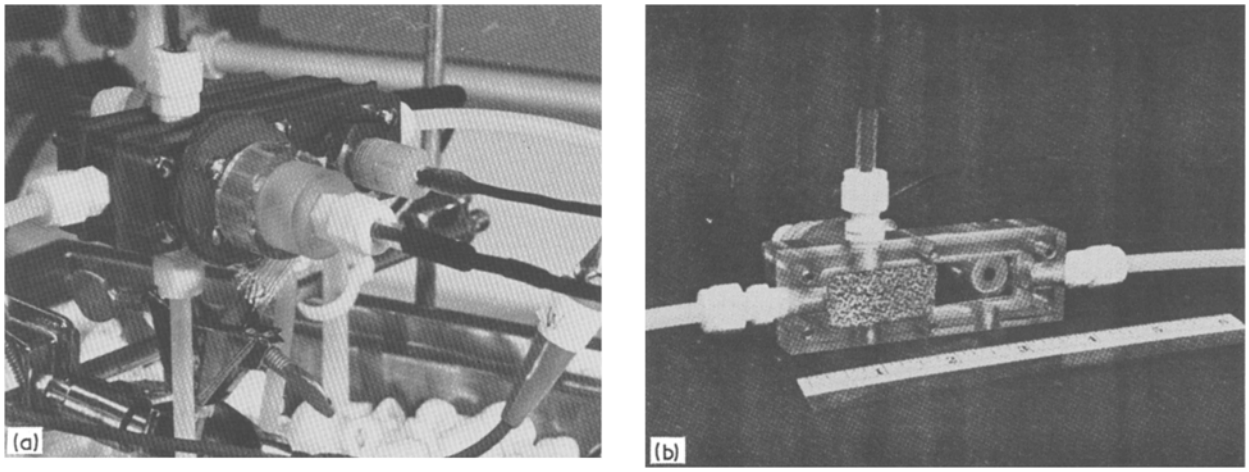

Fig. 2. Electrochemical cell. (a) View of cell placed in flow loop; (b) section of the electrochemical cell showing the platinized nickel foam collector electrode.

ing electrode port on the test cell. The exposed aluminium surface area is 0.283 cm^2. Figure 2a shows the epoxy-encapsulated aluminium working electrode on the right-hand side.

The counterelectrode is a nickel rod located in a chamber opposite the aluminium disc but separated from the flow channel by a Nafion-901® membrane. A Hg/HgO reference electrode contacts the electrolyte through a port at the bottom of the flow channel (Fig. 2b). The reference electrode is maintained at the cell temperature, to avoid any thermal junction contribution to the measured potential. Data for converting the potentials to the standard hydrogen scale are available from previous work [28].

The function of the monitoring section is to measure the rate of hydrogen evolution at the aluminium disc working electrode [23]. This is done by oxidizing the dissolved hydrogen in a porous collector electrode, which was fabricated from monolithic reticulated nickel (Fig. 2b). To ensure fast kinetics for the oxidation of hydrogen, the nickel foam was platinized at regular intervals, as previously described [23]. The monitoring section is equipped with a separate Hg/HgO reference electrode and a nickel counterelectrode for potentiostatic control. The counterelectrode chamber for the collector electrode is shown on the left-hand side of Fig. 2a.

This test cell design permitted study of the electrodissolution of aluminium and the effects of solution-phase inhibitors while simultaneously allowing separation of the anodic and cathodic partial currents that occur at the interface.

2.2. *Solutions*

Inhibitor solutions of varying compositions were prepared in analytical reagent grade KOH (4 M) using deionized and distilled water. Total solution volume for each experiment was 400 ml; a fresh solution was prepared for each test. When solutions were changed between experiments, a residual amount of solution (~ 25 ml) always remained in the pump reservoir. Accordingly, the system was flushed a minimum of five times with 4 M KOH to ensure thorough removal of the previous solution. This residual volume results in an error in the final concentration values of the inhibitors (but not of the KOH), but it was not accounted for because of the difficulty of draining the pump reservoir after each experiment. However, the error was estimated not to exceed 7%, and an acceptable correction can be applied if necessary. Dilute H_2SO_4 (0.01 M) was periodically flushed through the loop as a general cleansing agent; this was followed by a water rinse and several KOH rinses.

All compounds, except $Ga(OH)_3$ and K_2MnO_4, were commercially available. $Ga(OH)_3$ was prepared by dissolving 5 g of gallium (III) nitrate hydrate ($Ga(NO_3) \cdot 3.9\ H_2O$, 99.9%) in 100 ml deionized and distilled water, and titrating to a pH of 7.6 with KOH. The resultant fine precipitate was separated from the solvent by centrifugation, washed three times with distilled water and then dried in an oven overnight at 75° C.

Potassium manganate (K_2MnO_4) was prepared by adding 10 g $KMnO_4$ to 30 g KOH in 50 ml water and boiling until a clear green solution was obtained. The flask was then set in ice until a precipitate formed. The black-green crystals were collected by filtration, washed with 1 M KOH, and dried [29].

Gallium and indium were added as the hydroxide species ($Ga(OH)_3$ and $In(OH)_3$) and bismuth, tin and manganese were added as the oxyacid salts ($NaBiO_3$, Na_2SnO_3 and K_2MnO_4, respectively). All compounds readily dissolved in 4 M KOH, with the exception of $In(OH)_3$, which required heating for dissolution to occur.

2.3. *Experimental technique*

Before each experiment, the aluminium electrode surface was polished with 400- and 600-grit SiC paper and then with 0.3 and 0.05 μm alumina powder on microcloth. The surface was thoroughly rinsed with deionized water, then with ethanol and finally with deionized and distilled water. The working electrodes

® Registered Trademark of Dupont de Nemours, Inc.

were placed in a beaker of deionized and distilled water and sonicated for approximately 2 min to remove any residual particles from the surface. A new aluminium specimen was used for each experiment.

The electrolyte was placed in the reservoir and allowed to equilibrate at 50° ± 1° C for a minimum of 1 h before an experiment was started while simultaneously being sparged with pure nitrogen at a flow rate of $0.0321 s^{-1}$ (at STP). The solution was continuously sparged for the duration of the experiment to prevent buildup of hydrogen in the system. At the end of the equilibration period, the aluminium working electrode was inserted into the test cell and equilibrated under open circuit conditions for another hour. A potential of −0.5 V was applied (using Thompson Electrochem Microstat) to the precalibrated monitoring section during this time [23–26]. The final open circuit potential of the aluminium specimen was recorded at the end of this period.

The recorded open circuit potential was applied to the test specimen using an EG&G Model 362 potentiostat and then slowly decreased (to prevent overload) to −2000 mV (against Hg/HgO, 4 M KOH). The potential was then increased in a stepwise manner in the positive direction, and current readings were taken after each 25 mV increment. The currents from the test section and from the monitoring section were allowed to stabilize and then were read as the voltage dropped across standard resistors. The stabilization time varied from run to run, but was usually between 10 and 30 min. The potential range over which the measurements were obtained was −2.0 to −1.2 V (against Hg/HgO, 4 M KOH) as established in our previous work [23, 24].

The current/voltage curves reported in this work have been corrected for the uncompensated resistance between the working and reference electrodes, as previously described [23–26]. Briefly, the uncompensated resistance (R_u) was determined as the high frequency intercept of the impedance locus on the real axis, which gave $R_u = 1.0\,\Omega$. The polarization curves were then corrected by subtraction IR_u from the applied potentials, where I is the observed current.

3. Results

3.1. *Dissolution of aluminium in 4 M KOH*

Duplicate delineated current/voltage curves for aluminium in 4 M KOH at 50° C are shown in Fig. 3. These plots demonstrate the reproducibility achieved in this work, which was generally within ±10% for the current at any given potential, provided that the experiments were performed in an identical manner.

As observed previously [23, 24] aluminium is a passive metal in 4 M KOH at 50° C. This passivity is clearly shown in Fig. 3 by the existence of a passive region in which the anodic partial current is nearly independent of potential from −1.9 to −1.65 V, as well as by the tail end of an active–passive transition at −2.0 to −1.95 V. At voltages more positive than −1.65 V, the current increases nearly linearly with potential, which indicates the existence of a transpassive film of constant (potential-independent) resistance. In this respect, aluminium resembles zinc in alkaline environment [30], although we have not observed the current oscillations in the Al/OH^- system that are characteristic of the Zn/OH^- system at high potentials.

A kinetic model for the electrochemistry of aluminium in KOH solutions, that accounts very well for the impedance characteristics over wide ranges of applied potential and frequency was developed [25]. The essence of this model is that aluminium electrodissolution occurs via the stepwise addition of hydroxide ions to reactive centres and ultimately results in a fully

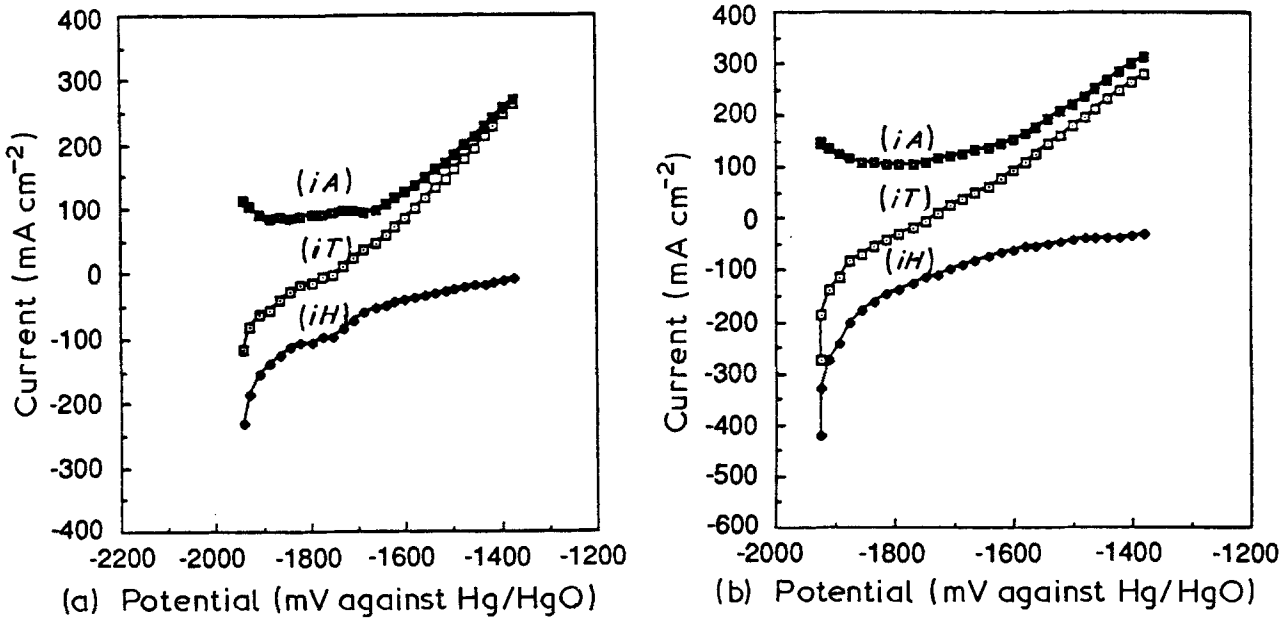

Fig. 3. Duplicate steady-state polarization curves for pure aluminium in 4 M KOH at 50° C, showing the total current (iT) and both anodic (iA) and cathodic (iH) partial currents.

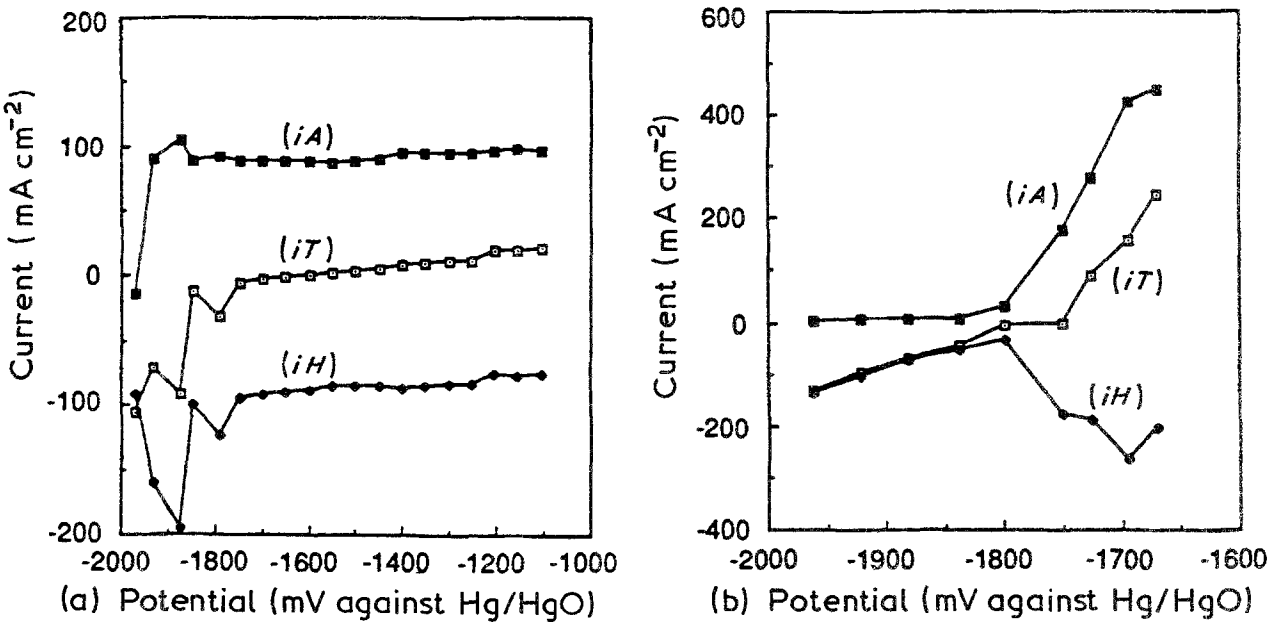

Fig. 4. Steady-state polarization curves for pure aluminium in KOH at 50°C, showing the total current (iT) and both anodic (iA) and cathodic (iH) partial currents. (a) [KOH] = 1 M, (b) [KOH] = 8 M.

coordinated surface species, $Al(OH)_3$, which then dissolves chemically as $Al(OH)_4^-$. The electrodissolution mechanism is coupled to hydrogen evolution (which is significant over the entire potential range of interest, see Fig. 3) by competition for surface sites. In the simulations of the impedance data [25], we had to assume that the surface concentration of active sites varied in a manner paralleling the anodic partial current (iA) shown in Fig. 3. Furthermore, the concentration (mol cm^{-2}) required for the simulations corresponds to many monolayers, which suggest that the surface is covered by a porous macroscopic film over the entire potential range of interest. The picture which emerges is that the surface is covered by a porous film of porosity which mimics the anodic current/voltage curve, and that the passivating reactions involving the stepwise adsorption of OH^- occur at the base of the pores. The existence of a macroscopic hydroxide/oxide film on aluminium in alkaline environments has been detected by a number of workers [31–3].

The concentration of hydroxide ion in the solution was found to have a strong effect on the electrochemical behaviour of aluminium in KOH, as shown in Figs 3 and 4. At low (1 M) hydroxide concentrations (Fig. 4a), both the hydrogen partial reaction and the aluminium

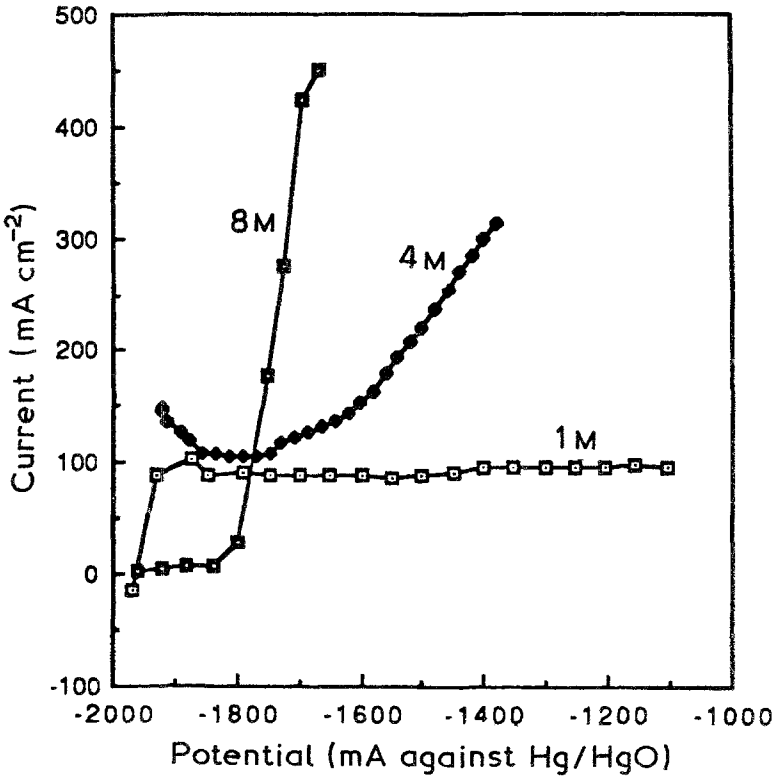

Fig. 5. Comparison of the partial anodic curves for aluminium in 1 M, 4 M and 8 M KOH at 50°C.

electrodissolution reaction are independent of potential over a wide range of voltages, from -1.85 to -1.1 V. Although the total current is small, the anodic dissolution partial current is large ($\sim 100\,mA\,cm^{-2}$) and is of the same order as that observed in the passive region for a higher (4 M) KOH concentration (see Fig. 3). Indeed, the region of potential-independent current observed in Fig. 4a corresponds to a greatly expanded passive region that was originally detected in the 4 M KOH solution in our previous work [23]. At a still higher KOH concentration (Fig. 4b), the passive region is considerably reduced, with the onset of transpassive dissolution being detected at -1.8 V. The transition to the transpassive state is accompanied by a marked increase in the rate of hydrogen evolution and hence in the rate of corrosion of the metal under discharge conditions.

The effect of hydroxide concentration on the electrodissolution of aluminium is shown more explicitly by comparing the anodic partial current/voltage curves in Fig. 5. Clearly, $[OH^-]$ has an enormous effect on the dissolution behaviour of aluminium in the transpassive region, with the current at any given potential increasing strongly with increasing hydroxide concentration. On the other hand, the reverse is observed in the passive region, particularly when the hydroxide concentration is increased from 4 M to 8 M (see Fig. 5). In this case, the passive current is found to decrease to a very small value ($< 10\,mA\,cm^{-2}$) at potentials more negative than -1.82 V.

The data contained in Figs 3–5 show that hydroxide ion inhibits aluminium electrodissolution in the passive range but catalyses the reaction in the transpassive region. Although the data are not extensive enough to provide a detailed mechanistic explanation of these phenomena, our findings have important practical implications for aluminium/air battery technology. Thus, provided that hydrogen evolution in the transpassive region can be inhibited by the addition of suitable alloying elements to the metal or inhibitors to the electrolyte, considerable advantages may exist in operating Al/air batteries at very high KOH concentrations. With these high KOH concentrations, advantage can be taken of the lower corrosion current under standby and the faster kinetics of discharge in the transpassive region.

3.2. *Solution-phase inhibition*

The current/voltage curves for aluminium in the presence of various solution-phase inhibitors were significantly less reproducible than in the presence of uninhibited solutions. Nevertheless, the data were sufficiently reproducible that important trends could be discerned as a function of inhibitor type and concentration. In this work, we were especially concerned with the mechanism of inhibition, in particular whether the inhibitor affected the partial anodic reaction, the cathodic reaction, or both. Our goal was to identify solution-phase inhibitors that kinetically hinder the cathodic reaction alone, because such inhibitors would have the effect of reducing the open circuit corrosion rate without affecting the discharge characteristics. Also, cathodic inhibition alone causes the open circuit potential (OCP) to be displaced in the negative direction and thus results in an apparent increase in the power density of the anode. However, this latter effect is an illusion because it is the power density under discharge, which is dominated by the partial anodic reaction, that is the important characteristic of the fuel.

3.2.1. Single-component inhibitor systems

3.2.1.1. Stannate. Previous studies have shown that stannate ion (SnO_3^{2-}) inhibits the corrosion of aluminium in hydroxide solutions, and the early work of Cooper *et al.* [1, 2] and others [34] employed this species to inhibit fuel corrosion in aluminium/air test cells. However, to our knowledge, the only previous studies of the mechanism of inhibition have been the brief impedance analyses of Macdonald *et al.* [35], who concluded that SnO_3^{2-} is reduced to metallic tin to form a porous deposit on the surface.

This work (Fig. 6) demonstrates that stannate inhibits both the anodic and cathodic partial reactions at the open circuit potential, with the former dominating at very high concentrations (Fig. 6c). These observations are consistent with the reduction of SnO_3^{2-} by the more electronegative aluminium to form a porous metallic deposit on the surface. At high (positive) potentials for the most concentrated stannate solution (Fig. 6c), the current is observed to increase sharply with increasing potential. The increase in current cannot be due to oxidation of the deposited tin, because the potential at which this process could occur is far more positive (-1.13 V against Hg/HgO, 4 M KOH [36]). Instead, the mechanism probably involves undermining of the deposited tin by aluminium dissolution, which ultimately leads to decohesion of the deposit from the surface. The experiments with stannate always results in the formation of colloidal tin suspended in the aqueous phase.

The explanation offered above is supported by the behaviour of the hydrogen evolution current. Thus, as the potential is made more positive ($E > -1.7$ V), the cathodic current *increases* to ultimately match that observed for the stannate-free system (Fig. 3). The increase in the hydrogen evolution current implies an increase in corrosion rate under discharge conditions, which can only lead to a lower efficiency of anode utilization. For this reason, we do not consider stannate alone to be a viable solution-phase inhibitor system for practical aluminium/air batteries.

3.2.1.2. Gallium. Gallium is an important component of many alloys that have been investigated as potential fuels for alkaline aluminium/air batteries. Accordingly, there has been considerable interest in studying the effect of $Ga(OH)_4^-$ on the electrodissolution of aluminium in alkaline media. However, we found that corrosion so dominates the chemistry of the interface that the aluminium specimen was completely consumed

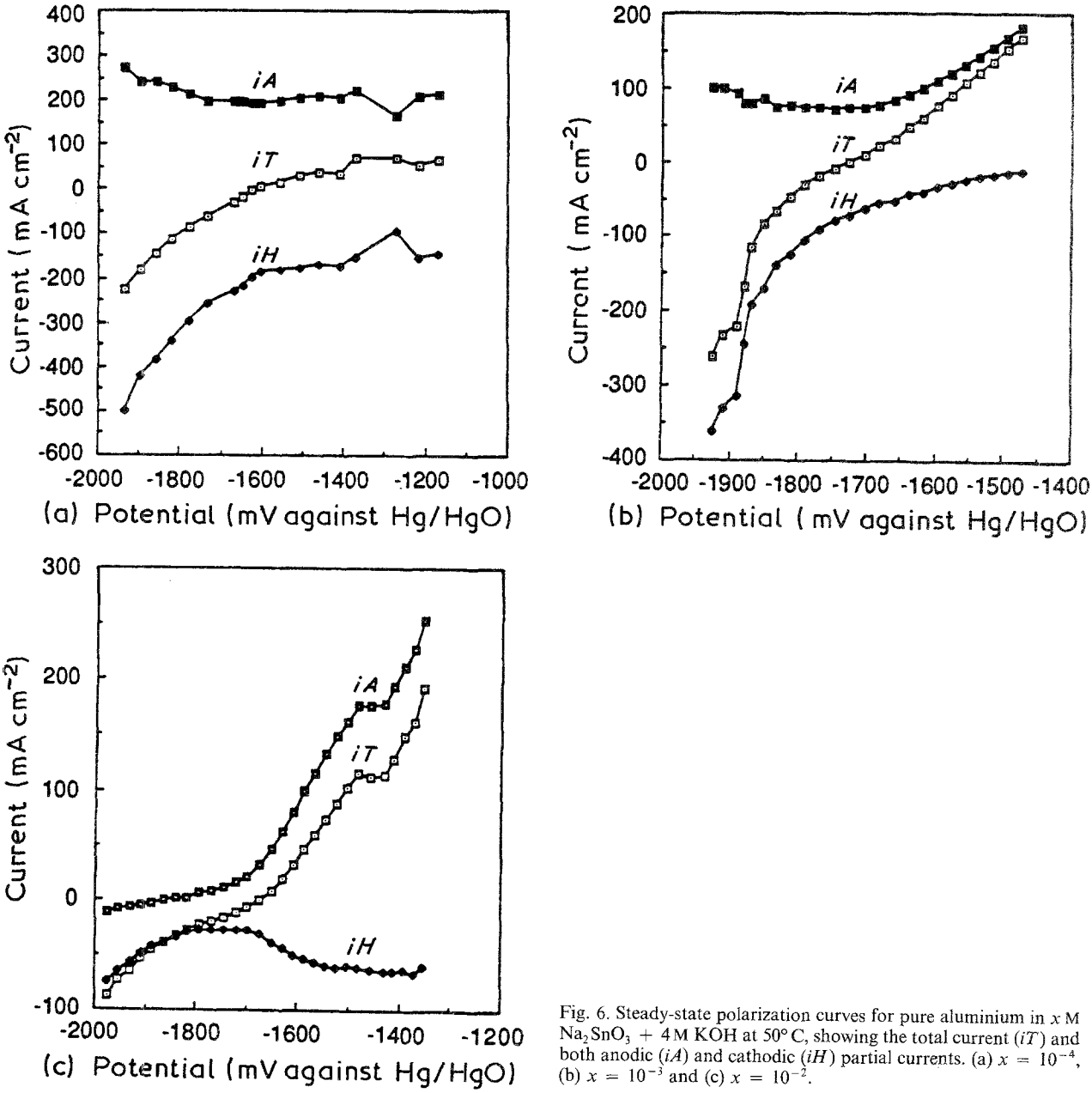

Fig. 6. Steady-state polarization curves for pure aluminium in x M Na_2SnO_3 + 4 M KOH at 50° C, showing the total current (iT) and both anodic (iA) and cathodic (iH) partial currents. (a) $x = 10^{-4}$, (b) $x = 10^{-3}$ and (c) $x = 10^{-2}$.

upon completion of an experiment. This observation clearly demonstrates the non-viability of gallate as a solution-phase inhibitor.

3.2.1.3. Indium. Indium is also a common alloying element is alloy fuels for alkaline aluminium/air batteries and, in fact, is an important alloying component of Alloy BDW® (Al–Mg–0.1In–0.2Mn), which has received so much attention over the past few years. Delineated current/voltage curves for aluminium in 4 M KOH with various concentrations of $In(OH)_3$ are shown in Fig. 7. At all concentrations, a sharp increase occurs in both the anodic and cathodic partial currents as the potential is increased from the passive zone in the positive direction. At still higher potentials, the surface passivates, with the results that there is a sudden decrease in both iA and iH to values that are typical of aluminium in pure 4 M KOH (Fig. 3). These observations strongly suggest that indium interferes with the normal passivating reactions on the aluminium surface, possibly by forming a deposit of metallic indium. This explanation is viable if we assume that hydrogen evolution is a much faster reaction on indium that it is on passive aluminium and thereby supports a greatly enhanced aluminium dissolution current in the presence of the metallic indium film. As the potential is made still more positive, the indium film becomes unstable, presumably because of undercutting of the aluminium as in the case of stannate. At sufficiently positive potentials ($E > -1.5$ V), the deposited indium is removed from the surface and the surface reactions are characteristic of those that occur on aluminium alone. Note that the equilibrium potential for $In/In(OH)_3$ is ~ -1.10 V (against Hg/HgO, 4 M KOH) [36], so that oxidative removal of indium from the surface does not appear to be a viable explanation for the decrease in iA and iH at high potentials. The existence of high corrosion currents at intermediate potentials renders $In(OH)_3$ alone unsuitable as a solution-phase inhibitor.

® Registered Trademark of ALCAN Ltd.

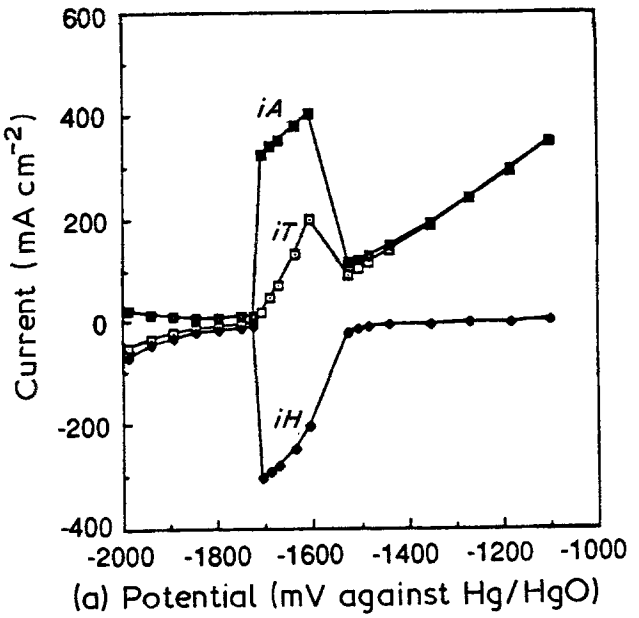

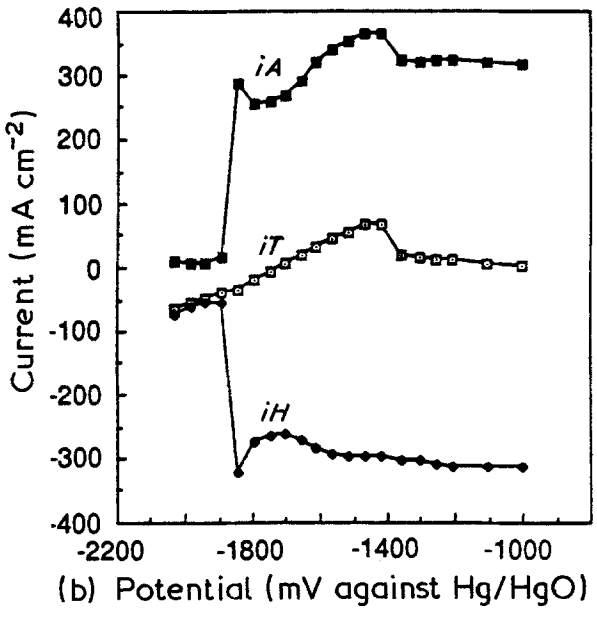

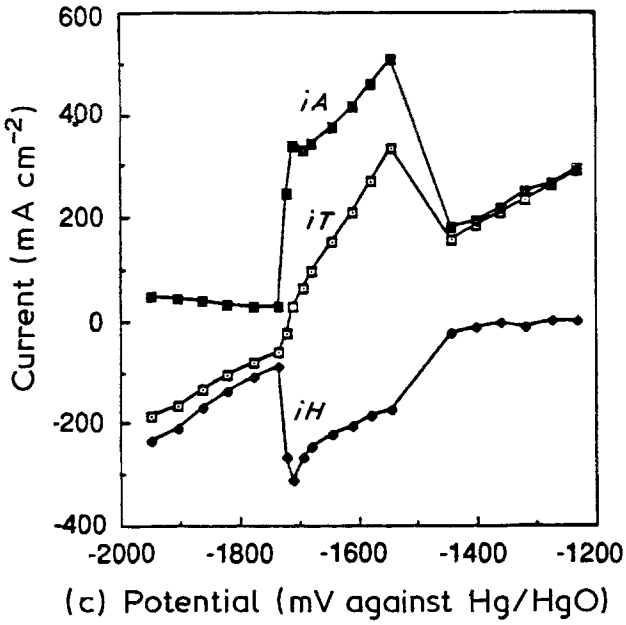

Fig. 7. Steady-state polarization curves for pure aluminium in x M $In(OH)_3$ + 4 M KOH at 50° C, showing the total current (iT) and both anodic (iA) and cathodic (iH) partial currents. (a) $x = 10^{-4}$, (b) $x = 10^{-3}$ and (c) $x = 10^{-2}$.

3.2.1.4. Manganese. Alloy BDW® (Al–1Mg–0.1In–0.2Mn) contains manganese as an alloying element in addition to indium and magnesium. The lowest oxyanion of manganese (ignoring the possible existence of $Mn(OH)_3^-$) is manganate (MnO_4^{2-}), in which the manganese atom is in the +6 oxidation state. The equilibrium potentials for the Mn/MnO_4^{2-} (10^{-3} M) and MnO_2/MnO_4^{2-} couples in 4 M KOH at 50° C are estimated [28, 36] from thermodynamic data to be approximately −0.49 and +0.34 V (against Hg/HgO), respectively, so manganate might be expected to be reduced to insoluble products (Mn or MnO_2) and hence act as an effective inhibitor of aluminium corrosion in alkaline media. However, these same data suggest that activation by oxidation of Mn or MnO_2 to MnO_4^{2-} will not occur at potentials of interest in this work, although activation by the formation of $HMnO_2^-$ is possible because the equilibrium potential for the $Mn/HMnO_2^- \equiv [Mn(OH)_3^-]$ couple is estimated to be about −1.7 V (against Hg/HgO) [36].

Typical delineated current/voltage curves for aluminium in 10^{-3} M K_2MnO_4 + 4 M KOH and in 10^{-2} M K_2MnO_4 + 4 M KOH solutions at 50° C are shown in Fig. 8. At potentials more positive than −1.7 V, the hydrogen evolution current is greatly reduced (especially for the lowest K_2MnO_4 concentration) and the observed current (iT) is due almost entirely to alloy dissolution. Comparison of Figs 3 and 8 indicates that some inhibition of the anodic current occurs, as would be expected if a thin layer of reaction product (possibly MnO_2) exists at the surface, but comparison of manganate with stannate for equivalent concentrations (Fig. 6) indicates that manganate is a more effective solution-phase inhibitor for aluminium/air battery applications, particularly at low concentrations (such as 10^{-3} M). Indeed, the effectiveness of manganate in inhibiting hydrogen evolution is such that it should be evaluated in aluminium/air cells.

The data given in Fig. 8b for the highest K_2MnO_4 concentration investigated in this work show that, for

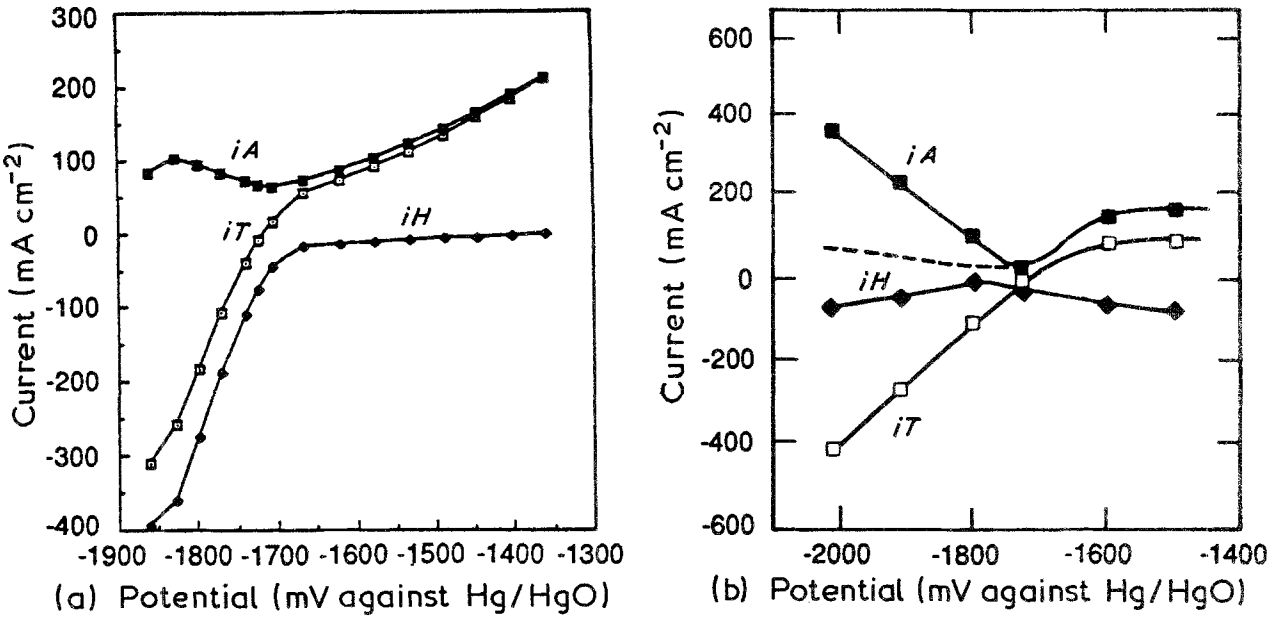

Fig. 8. Steady-state polarization curves for pure aluminium in x M K_2MnO_4 + 4 M KOH at 50° C, showing the total current (iT) and both anodic (iA) and cathodic (iH) partial currents. (a) $x = 10^{-3}$ and (b) $x = 10^{-2}$; - - - corrected anodic dissolution current (iA).

potentials more negative than − 1.75 V, the total current (that is, that observed in the external circuit) is more negative than the hydrogen evolution current. A similar phenomenon is observed in the case of stannate solutions (see Fig. 6c), although to a much smaller extent. This phenomenon coincides with a gradual change in the colour of the solution from green (MnO_4^-) to light brown (MnO_2). The colour change results from the reaction

$$MnO_4^{2-} + 2H_2O + 2e^- \longrightarrow MnO_2 + 4OH^- \quad (1)$$

which occurs in parallel with hydrogen evolution to form colloidal MnO_2 (brown). Reaction 1 also accounts for the additional cathodic reaction that results in the reversal of the relative magnitudes of iH and iT depicted in Fig. 8b. It is important to note that the electrodissolution current (iA) is calculated from iH and iT, with the assumption that hydrogen evolution is the only cathodic reaction occurring at the surface. Accordingly, the iA values indicated in Fig. 8b for potentials in the cathodic region are artifactually too high. Noting that iT in the absence of Reaction 1 can never be more negative than iH, we place a probable upper limit on iA indicated by the broken line in Fig. 8b.

Bismuth is also an element that showed some promise as an alloying component for alloy fuels for aluminium/air batteries [23, 24], but it has proven to be completely ineffective as a solution-phase inhibitor.

3.2.2. Multi-component inhibitor systems. Our previous studies on the corrosion of aluminium alloys in alkaline media [22] demonstrated a synergistic effect between alloying elements in inhibiting hydrogen evolution, so it was of interest to determine whether these same effects occur in solution-phase inhibition.

3.2.2.1. $Ga(OH)_4^-$ + $In(OH)_3$. A combination of $Ga(OH)_4^-$ and $In(OH)_3$ is clearly ineffective as an inhibitor system because of the exceedingly high hydrogen evolution currents observed at potentials more positive than − 1.5 V (Fig. 9a). Clearly, this combination of solution-phase species destroys the passivity of aluminium, to such an extent that the hydrogen evolution current very quickly reaches the maximum that can be measured by the collector electrode. At these potentials, the specimen quickly dissolved. Similar results were obtained at a lower $Ga(OH)_4^-$ concentration (10^{-4} M), but at 10^{-5} M $Ga(OH)_4^-$ (+ 10^{-3} M $In(OH)_3$), the massive corrosion of the substrate evident in Fig. 9a did not occur. These observations are of considerable interest because Al–Ga–In was found in previous work [22–4] to be a promising alloy fuel.

3.2.2.2. K_2MnO_4 + $In(OH_3)$. Inhibitor systems containing K_2MnO_4 + $In(OH)_3$ were also investigated because of the promising characteristics of Alloy BDW®. At moderate concentrations of both components, the delineated current/voltage curves (Fig. 9b) are similar to those displayed by aluminium in the manganate solution alone (Fig. 8a), except that the currents are of greater magnitude in the multicomponent system. Further additions of $In(OH)_3$ increased the hydrogen evolution current still further, so that in solutions of $[In(OH)_3] > 10^{-2}$ M, the beneficial effect of MnO_4^- was no longer evident.

3.2.2.3. $NaBiO_3$ + Na_2SnO_3. Solutions containing 10^{-3} M $NaBiO_3$ + 10^{-2} M Na_2SnO_3 also displayed unexpected behaviour (Fig. 9c); in this case the hydrogen evolution current was found to be essentially independent of potential (as detected by the collector electrode) over a wide range of potentials, which resulted in the anodic dissolution partial current

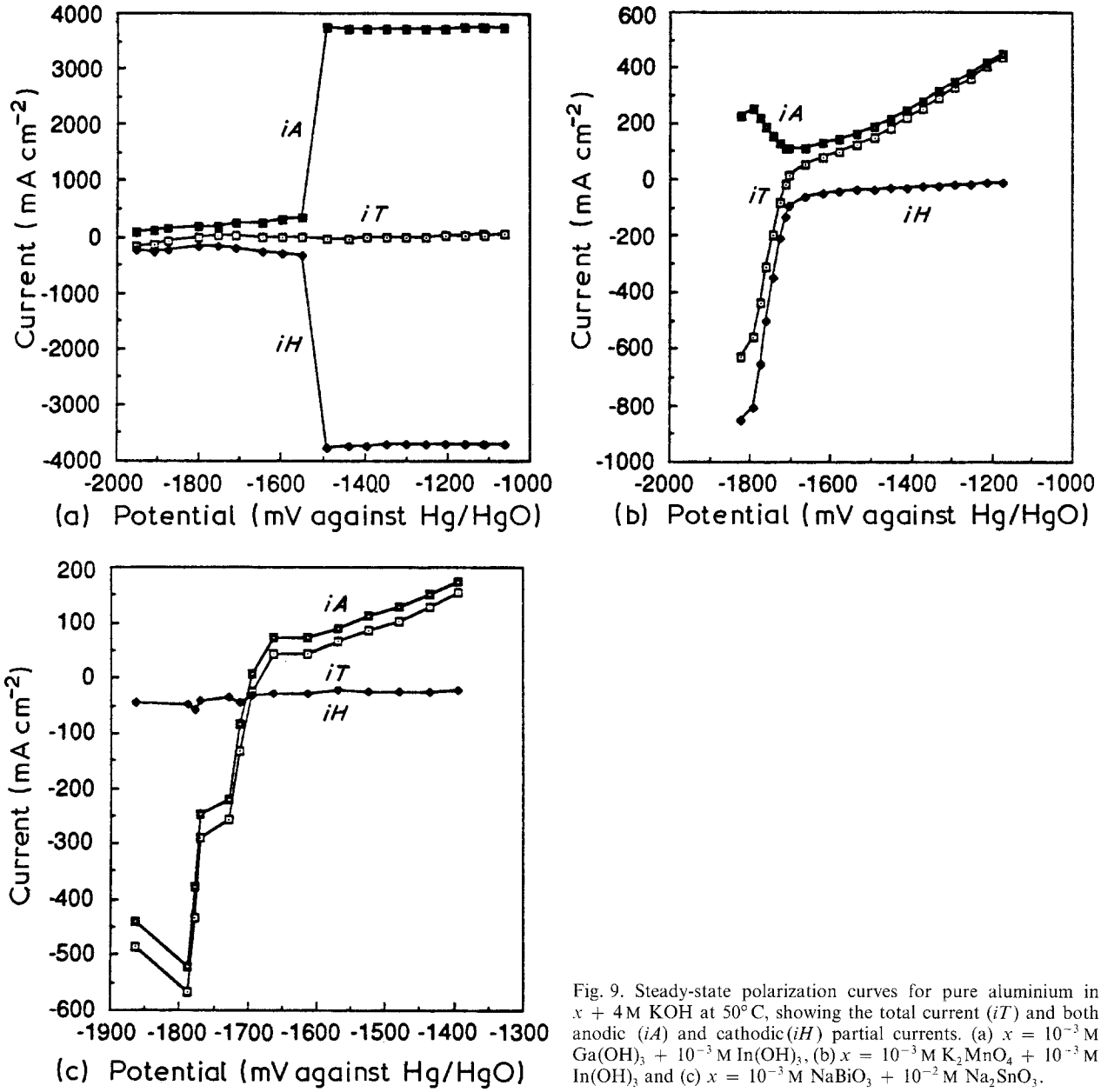

Fig. 9. Steady-state polarization curves for pure aluminium in x + 4 M KOH at 50° C, showing the total current (iT) and both anodic (iA) and cathodic (iH) partial currents. (a) $x = 10^{-3}$ M $Ga(OH)_3$ + 10^{-3} M $In(OH)_3$, (b) $x = 10^{-3}$ M K_2MnO_4 + 10^{-3} M $In(OH)_3$ and (c) $x = 10^{-3}$ M $NaBiO_3$ + 10^{-2} M Na_2SnO_3.

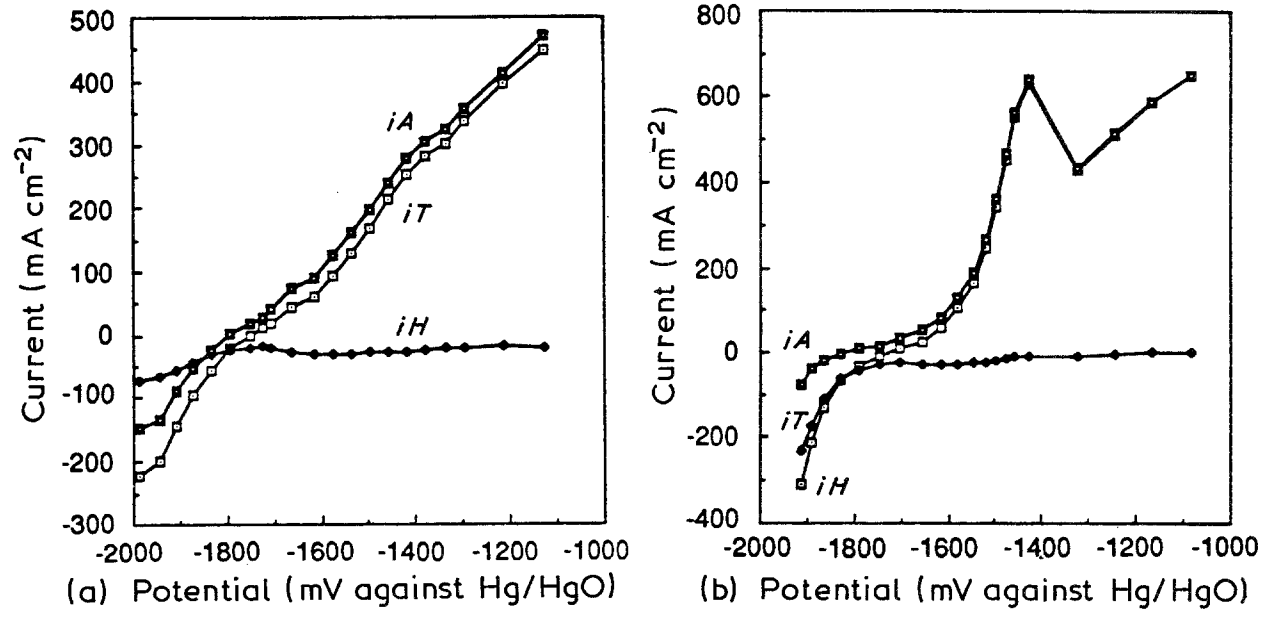

Fig. 10. Steady-state polarization curves for pure aluminium in 10^{-2} M Na_2SnO_3 + x M $In(OH)_3$ + 4 M KOH at 50° C, showing the total current (iT) and both anodic (iA) and cathodic (iH) partial currents. (a) $x = 10^{-3}$ and (b) $x = 10^{-2}$.

tracking the total current. At potentials more negative than −1.7 V, the anodic current became large and negative, presumably because of the reduction of stannate, bismuthate or both at the surface. However, the hydrogen evolution current was still substantial (30–50 mA cm^{-2}), so that BiO_3^- + SnO_3^{2-} is not considered to be a viable inhibitor system.

3.2.2.4. SnO_3^{2-} + $In(OH)_3$. The final multicomponent inhibitor system investigated in this work was SnO_3^{2-} + $In(OH)_3$. As shown in Fig. 10 this system results in moderate hydrogen evolution currents (5–25 mA cm^{-2}) for $E > E_{OCP}$ while allowing high discharge (dissolution) currents at reasonably negative voltages (iA = 600 mA cm^{-2} at −1.45 V). A passivation event at −1.45 to −1.35 V resembles that observed for Alloy BDW® [24]. However, unlike the case of Alloy BDW®, no concomitant response is observed in the hydrogen evolution current. When the $In(OH)_3$ concentration was decreased, the passivation event was no longer observed and there was a substantial decrease in the anodic partial current at any given potential. Clearly, $In(OH)_3$ has an activating effect on the dissolution of aluminium in this medium, but the expected increase in the hydrogen evolution current (compare with Fig. 7) is effectively countered by the stannate addition. The Na_2SnO_3 + $In(OH)_3$ system must be considered highly promising for practical aluminium/air batteries.

4. Discussion

When assessing the performance of fuels for aluminium/air batteries, we are concerned with three parameters: the open circuit corrosion rate (i_{corr}^{ocp}), and the discharge voltage (E_D) and corrosion rate (i_{corr}^{D}) under a given load (current density in the external circuit). The open circuit corrosion rate determines the loss of fuel (self-discharge) during standby, and hence should be kept as low as possible. However, a moderately high open circuit corrosion rate might be tolerated in practice if the battery is drained during standby. The discharge voltage (E_D) and the corrosion rate (i_{corr}^{D}) under load (iT) are important because they define the operating characteristics of the fuel; the product $P_D = |E_D \cdot iT|$ is a measure of the power density (mW cm^{-2}) of the fuel, and $CE = iT/(iT + i_{corr}^{D})$ is a measure of the coulombic efficiency with which the fuel is used as the battery is being discharged. A superior fuel will have high values for both quantities.

Open circuit corrosion potentials (E_{corr}), open circuit corrosion rates (i_{corr}^{ocp}), and discharge parameters (E_D, i_{corr}^{D} at various discharge currents) for aluminium, Alloy BDW®, and Alloy 21 in alkaline and inhibited alkaline environments are summarized in Table 1. These data have been used to calculate the relative open circuit corrosion rates and the values for the power density (P_D) and coulombic efficiency (CE) listed in Table 2.

Not all of the 'inhibitors' investigated in this work reduced the corrosion rate of aluminium below that for aluminium in 4 M KOH. For example, with the addition of $In(OH)_3$, the corrosion rate increased by almost a factor of 3 (see Tables 1 and 2) under open circuit conditions and to much higher values under discharge conditions, with the result that coulombic efficiencies for fuel utilization were low (Table 2). The ability of $In(OH)_3$ to destroy the passivity of aluminium is clearly evident from the current/voltage curves shown in Fig. 7. A similar but much more intense effect was observed when $Ga(OH)_3$ was added to the electrolyte, resulting in complete destruction of the aluminium specimen.

Stannate ion (SnO_3^{2-}), when present at high concentrations, caused a substantial decrease in the open circuit corrosion current but still produced poor coulombic efficiency under discharge compared with that in the uninhibited environment. However, an Na_2SnO_3 concentration of 10^{-3} M, yielded a coulombic efficiency for a net discharge current of 200 mA cm^{-2} of 95%, whereas that for [Na_2SnO_3] = 10^{-2} M under similar conditions was only 77% and that for discharge at a net current of 100 mA cm^{-2} was 79%. The inhibi-

Table 1. Performance data for aluminium and aluminium alloys in alkaline and inhibited alkaline solutions at 50° C

Alloy	*Solution (+4 M KOH)*	E_{corr} (*V against Hg/HgO*)	i_{corr}^{ocp} (*mA cm*$^{-2}$)	E_D (*V against Hg/HgO*) + i_{corr}^{D}(*mA cm*$^{-2}$) *at iT of*		
				100 *mA cm*$^{-2}$	200 *mA cm*$^{-2}$	400 *mA cm*$^{-2}$
Al	–	−1.71	95	−1.56(43)*	−1.41(24)	–
Al	10^{-3} M Na_2SnO_3	−1.73	72	−1.54(26)	−1.44(10)	–
Al	10^{-2} M Na_2SnO_3	−1.68	31	−1.48(59)	−1.30(60)	–
Al	10^{-3} M $In(OH)_3$	−1.74	264	–	–	–
Al	10^{-2} M $In(OH)_3$	−1.73	280	−1.65(235)	−1.55(206)	–
Al	10^{-3} M K_2MNO_4	−1.73	65	−1.50(9.6)	−1.30(2.0)	–
Al	10^{-3} M K_2MnO_4 + 10^{-3} M $In(OH)_3$	−1.71	100	−1.55(42)	−1.32(29)	−1.10(15)
Al	10^{-3} M K_2MnO_4 + 10^{-2} M $In(OH)_3$	−1.70	70	−1.40(44)	−1.10(30)	–
Al	10^{-2} M Na_2SnO_3 + 10^{-3} M $In(OH)_3$	−1.72	19	−1.55(31)	−1.40(27)	−1.10(18)
Al	10^{-2} M Na_2SnO_3 + 10^{-2} M $In(OH)_3$	−1.75	26	−1.5(27)	−1.47(24)	−1.38(17)
BDW® (Al–1Mg–0.1In–0.2Mn)		−1.80	5	−1.65(25)	−1.57(60)	−1.46(80)
21 (Al–0.2Ga–0.1In–0.1Tl)		−1.64	4.6	−1.35(<1)	–	–

* Values in parentheses are i_{corr}^{D} in mA cm^{-2}.

Table 2. Power densities and coulombic efficiencies for aluminium and aluminium alloys in alkaline and inhibited alkaline solutions at 50° C

Alloy	*Solution*	$i^{o}_{corr}/i^{ocp}_{corr}(Al)$	P_D *and* (CE) *at a discharge current of*		
			100 $mA\ cm^{-2}$	200 $mA\ cm^{-2}$	400 $mA\ cm^{-2}$
Al	–	1.00	156(0.70)†	282(0.89)	ND
Al	10^{-3} M Na_2SnO_3	0.76	154(0.79)	288(0.95)	ND
Al	10^{-2} M Na_2SnO_3	0.33	148(0.63)	260(0.77)	ND
Al	10^{-3} M $In(OH)_3$	2.78	NA*	NA	NA
Al	10^{-2} M $In(OH)_3$	2.95	165(0.30)	310(0.49)	NA
Al	10^{-3} M K_2MnO_4	0.68	150 (0.91)	260 (0.99)	ND
Al	10^{-3} M K_2MnO_4 + 10^{-3} M $In(OH)_3$	1.05	155(0.70)	264(0.87)	440(0.96)
Al	10^{-3} M K_2MnO_4 + 10^{-2} M $In(OH)_3$	0.74	140(0.69)	220(0.87)	ND
Al	10^{-2} M Na_2SnO + 10^{-3} M $In(OH)_3$	0.20	155(0.76)	280(0.88)	440(0.96)
Al	10^{-2} M Na_2SnO_3 + 10^{-2} M $In(OH)_3$	0.27	155(0.79)	294(0.89)	552(0.96)
BDW (Al–1Mg–0.1In–0.2Mn)		0.05	165(0.80)	314(0.77)	584(0.83)
21 (Al–0.2Ga–0.1In–0.1Tl)		0.048	135(> 0.99)	ND*	ND

* NA = Not achieved; ND = not determined.
† Values in parentheses are coulombic efficiencies (CE).

tive effect of stannate ion on aluminium corrosion under open circuit conditions has been documented (by Cooper *et al.* [1, 2]), but its effect on the coulombic efficiency of aluminium in hydroxide media under discharge conditions had not been previously characterized.

Of the single-component inhibitor systems explored in this work, that containing potassium manganate (K_2MnO_4) was the most effective. At a concentration of 10^{-3} M, which is considered to be practical in operating batteries, the coulombic efficiency of the aluminium anode was found to exceed 90% for discharge currents of 100 and 200 mA cm^{-2}, with the efficiency for the highest discharge rate being 99%. However, the open circuit current was less than a factor of 2 smaller than that of the inhibitor-free system (see Table 2), so that standby corrosion is not strongly inhibited.

For the four binary inhibitor systems listed in Table 2, the best performance was displayed by the stannate + indium hydroxide systems, which yield open circuit corrosion rates that are factors of 4 to 5 lower than those of uninhibited solutions and display coulombic efficiencies as high as 96% for a net discharge current of 400 mA cm^{-2}. Indeed, the coulombic efficiencies exhibited by these systems at the two highest discharge rates (200 and 400 mA cm^{-2}) are substantially higher than those observed for Alloy BDW®, which is a leading candidate fuel for aluminium/air batteries, but are still only marginally better than those for aluminium in uninhibited 4 M KOH. Clearly, the only substantial benefit of the inhibitors in these cases is suppression of the open circuit corrosion rate. Alloy BDW® exhibits a much lower open circuit corrosion rate than does aluminium in either the inhibited or uninhibited enrivonments, but the coulombic efficiency performance of Alloy BDW® under discharge is not substantially better than that of aluminium, which indicates that alloying benefits only the standby performance in this particular case. Only Alloy 21, the thallium-containing alloy, matches Alloy BDW® in its standby corrosion characteristics (Table 2), but the discharge voltage for Alloy 21 is significantly more positive (and hence the power density is lower) than that for Alloy BDW®. Insufficient data are available to determine the coulombic efficiency of Alloy 21 under high rate discharge ($iT \geqslant 200$ mA cm^{-2}) conditions, but extrapolation of the data contained in [24] indicates that the coulombic efficiency would be very high (essentially equal to 100%).

Finally, the data listed in Table 2 show that Alloy BDW® exhibits the highest power densities of any system at all the discharge rates considered in this work, because of the more negative discharge voltages exhibited by this alloy. However, previous work [24] indicated that Alloy BDW® may exhibit a secondary passivation phenomenon at high potentials, in which case the power density approaches that for pure aluminium.

5. Summary and conclusions

The discharge characteristics of aluminium in 4 M KOH and in inhibited 4 M KOH solutions at 50° C have been explored. We found that potassium manganate (K_2MnO_4) and Na_2SnO_3 + $In(OH)_3$ are effective inhibitor systems, particularly at high discharge rates (400 mA cm^{-2}), but at low discharge rates only manganate offers a significant advantage in coulombic efficiency over that of the uninhibited solution. Alloy BDW® exhibits a very low open circuit (standby) corrosion rate, but its coulombic efficiency under discharge was found to be no better than that of aluminium in the same uninhibited solution. Alloy 21, however, exhibited a performance comparable to that of Alloy BDW® under open circuit conditions and a much higher coulombic efficiency at low discharge rate (100 mA cm^{-2}) conditions. The performance of Alloy 21 under high discharge rate conditions was not determined. Alloy 21 has the significant disadvantage that it contains thallium.

Acknowledgement

The authors gratefully acknowledge support of this work by the Department of Energy/Lawrence Berkeley Laboratory under Grant No. DE-AC03-76SF00098.

References

[1] J. F. Cooper, R. V. Homsky and J. H. Landrum, 'The aluminum–air battery for electric vehicle propulsion', in *Proceedings of the 15th Intersociety Energy Conversion Engineering Conference, June 1980*, Lawrence Livermore National Laboratory UCRL-84443, Livermore, California (1980).

[2] J. F. Cooper, R. V. Homsy, J. H. Landrum and S. P. Perone, 'The mechanically-refuelable aluminum–air battery', in *ibid.*

[3] S. P. Perone, N. Kirkman Bey and J. F. Cooper, 'Parametric study of an alkaline-electrolyte aluminum–air flow cell', in *ibid.*

[4] J. D. Salisbury, E. Behrin, M. K. Kong and D. J. Whisler, 'A Comparative Analysis of Aluminum–Air Battery Propulsion Systems for Passenger Vehicles', Lawrence Livermore National Laboratory, UCRL-52933, Livermore, California (1980).

[5] 'Aluminum–Air Battery System, Assessment of Technical and Market Viability for Electric Vehicle Application', Final Report to Brookhaven National Laboratory, Alvin J. Salkind Associates (1980).

[6] 'Control System Considerations for an Aluminium–Air Battery Powered Electric Vehicle', Final Report to Lawrence Livermore National Laboratory, William M. Brobeck and Associates (1980).

[7] A. R. Despic, *Recueil Des Travaux* **12** (1979) 1.

[8] H. B. Urgach and M. C. Cervi, 'Aluminum-based anodes for underwater fuel cells', *Proceedings of the 12th Intersociety Energy Conversion Engineering Conference* No. 1 (1977) p. 276.

[9] W. A. Bryant and E. S. Buzzelli, 'A comparison of metal–air batteries for electric vehicle propulsion', in *Proceedings of the 14th Intersociety Energy Conversion Engineering Conference*, No. 1, (1979) pp. 651–653.

[10] J. F. Cooper, 'Preliminary Design and Analysis of Aluminum–Air Cells Providing for Continuous Feed and Full Utilization of Anodes', DoE Report, UCID0-19178, Order No. DE81030479 (1981) p. 9.

[11] R. V. Homsy, 'Rapidly-Refuelable 167 cm^2 Aluminum–Air Power Cell', DoE Report, UCID-19244, Order No. DE82006251 (1981) p. 44.

[12] O. R. Brown and J. S. Whitley, *Electrochim. Acta* **32** (1987) 545.

[13] Y. Hori, J. Takaom and H. Shomon, *ibid.* **30** (1985) 1121.

[14] F. Dalard, J. Y. Macht, J. Guilton and J. C. Sohm, *ibid.* **21** (1976) 249.

[15] W. Bohnstedt, *J. Power Sources* **5** (1980) 245.

[16] W. Schneider and K. Wiesner, *Bull. Chem. Soc. Beeg.* **48** (1983) 5241.

[17] C. J. McMinn and J. A. Branscomb, 'Production of Anodes for Aluminum–Air Power Cells Directly from Hall Cell Metal', Report to DoE, Subcontract No. 6124909 (1981).

[18] A. R. Despic, D. M. Drazic, M. M. Purenovic and N. Cikovic, *J. Appl. Electrochem.* **6** (1976) 527.

[19] J. R. Moden and G. Perkons, US Patent No. 4,150,104 (1979).

[20] A. R. Despic, D. M. Drazic, M. M. Purenovic and N. Cikovic, *J. Appl. Electrochem.* **6** (1976) 527.

[21] S. Zecevic, L. Gajic, A. R. Despic and D. M. Drazic, *Electrochim. Acta* **26** (1981) 1625.

[22] D. D. Macdonald, K. H. Lee, A. Moccari and D. Harrington, *Corrosion* **44** (1988) 652.

[23] S. Real, M. Urquidi-Macdonald and D. D. Macdonald, *J. Electrochem. Soc.* **135** (1988) 2397.

[24] *Idem, ibid.* **135** (1988) 1633.

[25] D. D. Macdonald, S. Real, S. I. Smedley and M. Urquidi-Macdonald, *ibid.* **135** (1988) 2410.

[26] *Idem*, 'Development and Evaluation of Anode Alloys for Aluminum–Air Batteries', Final Report to Eltech Systems Corp., DoE Subcontract 100484-MLM (1987).

[27] M. Urquidi-Macdonald, S. Real and D. D. Macdonald, *J. Electrochem. Soc.* **133** (1986) 2018.

[28] B. G. Pound, R. P. Singh and D. D. Macdonald, *J. Power Sources* **18** (1986) 1.

[29] K. A. Jensen and W. Klemm, *Z. Anorg. Allg. Chem.* **237** (1938) 47.

[30] M. C. H. McKubre and D. D. Macdonald, *J. Electrochem. Soc.* **127** (1980) 632.

[31] K. E. Heusler and W. Allgaier, *Werkst. Korros.* **22** (1971) 297.

[32] O. R. Brown and J. S. Whitley, *Electrochim. Acta* **32** (1987) 545.

[33] R. Greef and C. F. W. Norman, *J. Electrochem. Soc.* **132** (1985) 2362.

[34] Eltech Systems Corp., private communication (1987).

[35] D. D. Macdonald, K-H. Lee, A. Moccari, D. Harrington and M. Urquidi, 'The Metallurgy and Electrochemistry of the Aluminum Anode', Final Report to ELTECH Systems Corp. from Ohio State University, FCC 5162 (1984).

[36] M. Pourbaix, 'Atlas of Electrochemical Equilibria', National Association of Corrosion Engineers Eng., Houston, TX (1974).